Desalination and Water Treatment
www.deswater.com
doi: 10.1080/19443994.2015.1120685

57 (2016) 21524–21533
September

Taylor & Francis
Taylor & Francis Group

Nanostructured adsorbent (MnO_2): Synthesis and least square support vector machine modeling of dye removal

Niyaz Mohammad Mahmoodi*, Zahra Hosseinabadi-Farahani, Hooman Chamani

Department of Environmental Research, Institute for Color Science and Technology, Tehran, Iran, Tel. +98 21 22969771; Fax: +98 21 22947537; emails: mahmoodi@icrc.ac.ir, nm_mahmoodi@aut.ac.ir, nm_mahmoodi@yahoo.com (N.M. Mahmoodi), zahrahof80@gmail.com (Z. Hosseinabadi-Farahani), chamani.hooman@yahoo.com (H. Chamani)

Received 14 March 2015; Accepted 7 November 2015

ABSTRACT

In this study, MnO_2 nanoparticle was synthesized by a simple method. Dye removal ability of the synthesized nanoparticle was investigated. Basic Blue 41 (BB41), Basic Red 46 (BR46), and Basic Red 18 (BR18) were used as model compounds. The structure of the synthesized adsorbent was characterized by scanning electron microscopy and Fourier transform infrared techniques. Least square support vector machine (LSSVM) was used to model the dye removal. The graphical plots and the values of statistical parameter showed LSSVM as an intelligent model suitable for modeling of dye adsorption. The effect of adsorbent dosage and initial dye concentration on dye removal was investigated. The kinetic and isotherm of the adsorption process were studied. The studies confirmed that the adsorption of BB41, BR46, and BR18 followed the Freundlich, Langmuir, and Freundlich isotherms, respectively. Adsorption kinetic of dyes was found to conform to pseudo-second-order kinetic model.

Keywords: Nanostructured adsorbent; Synthesis; Dye removal modeling; Least square support vector machine

1. Introduction

Water resources are an important part of our environment. Therefore, water pollution is a major global issue [1–5]. Among different pollutants, dyes are an important group because they are used in various industries such as paper, plastic, textile, food, cosmetic, and leather [6–9]. Some dyes and their intermediates are commonly toxic and harmful for our health. In addition to changing the color and appearance of the water, they disrupt activities of aquatic organisms such as photosynthesis [7,10,11]. In recent years, various techniques have been used for the removal of dyes from contaminated water (e.g. chemical oxidation, photodegradation, biological treatment, ozonation, and adsorption) [11–17]. Among them, adsorption process is considered as a simple, effective, and economical method. Various adsorbents were investigated for dye removal. Furthermore, finding a simple and inexpensive method for synthesis of adsorbent is important [5,6].

A literature review showed that the modeling of dye adsorption on MnO_2 nanoparticle using least square support vector machine (LSSVM) was not studied. In this paper, a simple method was used for synthesis of MnO_2 nanoparticle. The dye removal ability of MnO_2 nanoparticle was studied in single systems. Basic Blue 41(BB41), Basic Red 46 (BR46), and

*Corresponding author.

1944-3994/1944-3986 © 2015 Balaban Desalination Publications. All rights reserved.

Basic Red 18 (BR18) were used as cationic dyes. The characteristics of adsorbent were investigated by Fourier transform infrared (FTIR) and scanning electron microscopy (SEM). LSSVM was applied to model dye removal based on experimental data obtained from laboratory. The isotherm and kinetic of dye adsorption on the synthesized adsorbent were studied. The effect of operational parameters (adsorbent dosage and initial dye concentration) on dye removal was evaluated in details.

2. Materials and methods

2.1. Chemicals

Manganese nitrate·$4H_2O$ and sodium hydroxide were purchased from Merck. Cationic dyes (Basic blue 41, Basic red 46, and Basic red 18) were used as model dyes. The chemical structure of dyes is shown in Fig. 1.

2.2. Synthesis of MnO_2 nanoparticle

Sodium hydroxide (1 g) was dissolved in 90 mL distilled water. Manganese nitrate·$4H_2O$ (1 g) was added to the prepared solution. The resulting solution was stirred for 1 h. The bottle was sealed and placed in an oven at 120℃ for 24 h. Supernatant was then discarded and the remaining solid was washed using deionized water. The solid material was dried in an oven at 120℃ for 12 h. The functional groups of the synthesized adsorbent were studied using FTIR spectrum (Perkin-Elmer Spectrophotometer Spectrum One) in the range of 4,000–450 cm^{-1}. The morphological structure of the adsorbent was examined by SEM using LEO 1455VP scanning microscope.

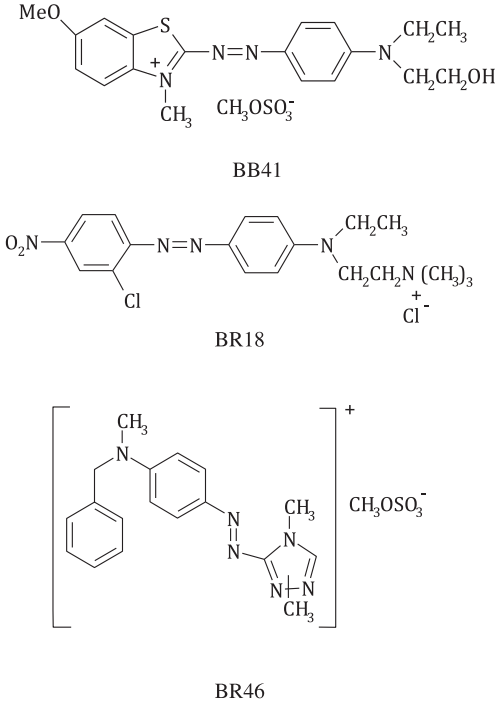

Fig. 1. Chemical structure of dyes.

2.3. Adsorption procedure

At room temperature, adsorbent was added to 250 mL of dye solution and stirred for 1 h. Solution was sampled at certain time intervals during the adsorption process. By centrifugation of the samples, adsorbent was settled and separated. The residual dye in the samples was determined using UV–vis Spectrophotometer (Perkin-Elmer Lambda 25 Spectrophotometer) at maximum wavelength of dyes. Maximum wavelength of BB41, BR18, and BR46 was 605, 488, and 531 nm, respectively.

The effect of adsorbent dosage on dye removal was investigated by contacting 250 mL of dye solution (20 mg/L) with different amounts of adsorbent at 25℃ for 1 h. Furthermore, the effect of initial dye concentration (20–80 mg/L) on dye removal was investigated by contacting 250 mL of dye solution with the adsorbent at 25℃ for 1 h.

3. Result and discussion

3.1. Characterization

The FTIR spectrum of MnO_2 nanostructure is shown in Fig. 2. The band at about 1,000 cm^{-1} can be attributed to υMn–O–H vibration [18]. The two peaks at 499 and 610 cm^{-1} arise from the stretching vibration of the Mn–O and Mn–O–Mn bonds [18,19]. The peaks of 1,600 and 1,000 cm^{-1} are assigned to the bending vibration of H_2O and OH, which implies that the hydroxyl groups existed in MnO_2 [19]. The peak at 3,434 cm^{-1} can be attributed to the stretching vibration of the water molecule and OH^- in the structure. The peak at 1,632 cm^{-1} is assigned to bending vibration of H_2O and OH^- [18–20]. The results clearly indicated that the MnO_2 samples were hydroxylated. The band at about 1,400 cm^{-1} is also ascribed to the bending vibrations of the O–H groups combined with manganese oxides [21].

SEM is applied as a suitable tool to determine surface morphology, shape, and size of particles. SEM of MnO_2 nanoparticle is shown in Fig. 3. As shown in the images, nanoparticles have a sphere shape.

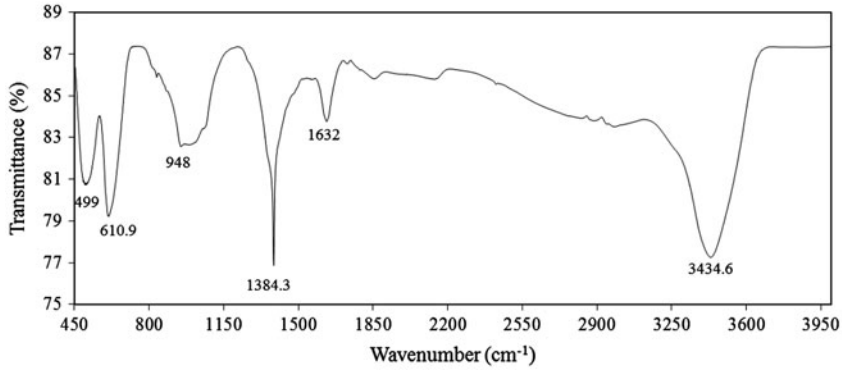

Fig. 2. FTIR spectrum of MnO_2 nanoparticle.

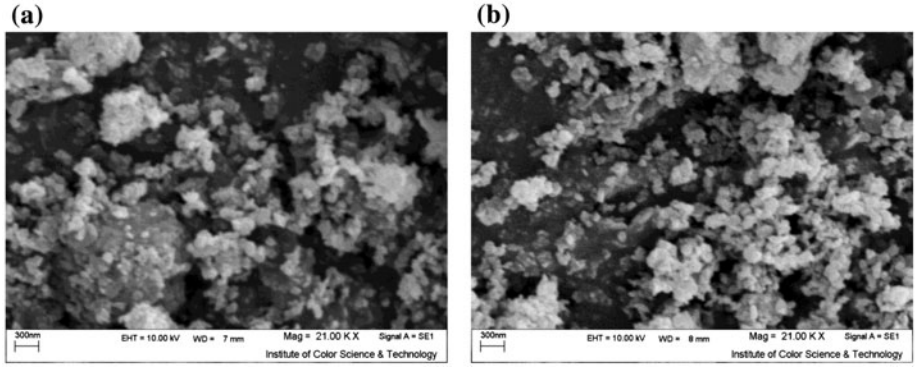

Fig. 3. SEM images of the synthesized MnO_2 nanoparticle.

3.2. LSSVM dye removal modeling

Support vector machine (SVM) was introduced by Vapnik [22]. SVM can be used for classification, nonlinear function, and density estimation lead to convex optimization problems, typically quadratic programming [23], which are often taking up a great deal of time and difficult to implement adaptively [24]. LSSVM uses a set of linear equations to minimize the complexity of optimization process, unlike SVM that utilizes quadratic programming problem [25–27]. More detailed information can be found in previous research [25], so the theory is not described here.

At the beginning, the experimental data were divided to two parts, training data-sets (70% of all data-sets) and testing data-sets (30% of all data sets). All data were normalized between −1 and 1. Table 1 represents ranges of experimental data. The model was developed for each dye using training data-sets and then it was checked through testing sets.

In order to develop the model, the free LSSVM toolbox (version 1.8, Suykens, Leuven, Belgium) was applied in MATLAB environment. In this modeling cross validation, simplex and RBF kernel were selected as cost function, optimization routine, and kernel function, respectively. The performance of modeling was evaluated using graphical plots and statistical parameter, coefficient of determination (R^2), which can be calculated using the following equation:

$$R^2 = 1 - \frac{\sum_{i=1}^{N} (y_{i,pred} - y_{i,exp})^2}{\sum_{i=1}^{N} (y_{i,exp} - \bar{y}_{exp})^2} \quad (1)$$

where N is the number of data points, $y_{i,pred}$ and $y_{i,exp}$ are the predicted and experimental y value of point i, respectively, and $\bar{y}_{exp}$ is the average of experimental values.

Table 1
Ranges of experimental data

Variable	Range		
	BB41	BR18	BR46
Input			
Adsorbent dosage (g)	0.025–0.15	0.05–0.2	0.15–0.3
Initial dye concentration (mg/L)	20–80	20–80	20–80
Adsorption time (min)	2.5–60	2.5–60	2.5–60
Output			
Dye removal (%)	0–100	0–100	0–100

As shown in Fig. 4, a good agreement can be seen between the predicted dye removal values by LSSVM and experimental ones. According to this figure, the data points are distributed in a thin area around $y = x$ line. It means that experimental and the predicted values are similar to a large extent. As a result, based on graphical plots and the values of R^2 (Table 2), LSSVM was appropriate as a powerful tool for modeling of adsorption process in our system.

Table 2
Coefficient of determination values

Dye	R^2 train	R^2 test
BB41	0.9978	0.9927
BR46	0.9984	0.9949
BR18	0.9933	0.9876

The plots of dye removal (%) vs. time (min) at different adsorbent dosages are shown in Fig. 5. The increase in dye adsorption with adsorbent dosage can be attributed to increased adsorbent surface and the availability of more adsorption sites. However, if the adsorption capacity is expressed in milligrams of adsorbate per gram of adsorbent, the capacity decreases with the increasing amount of adsorbent.

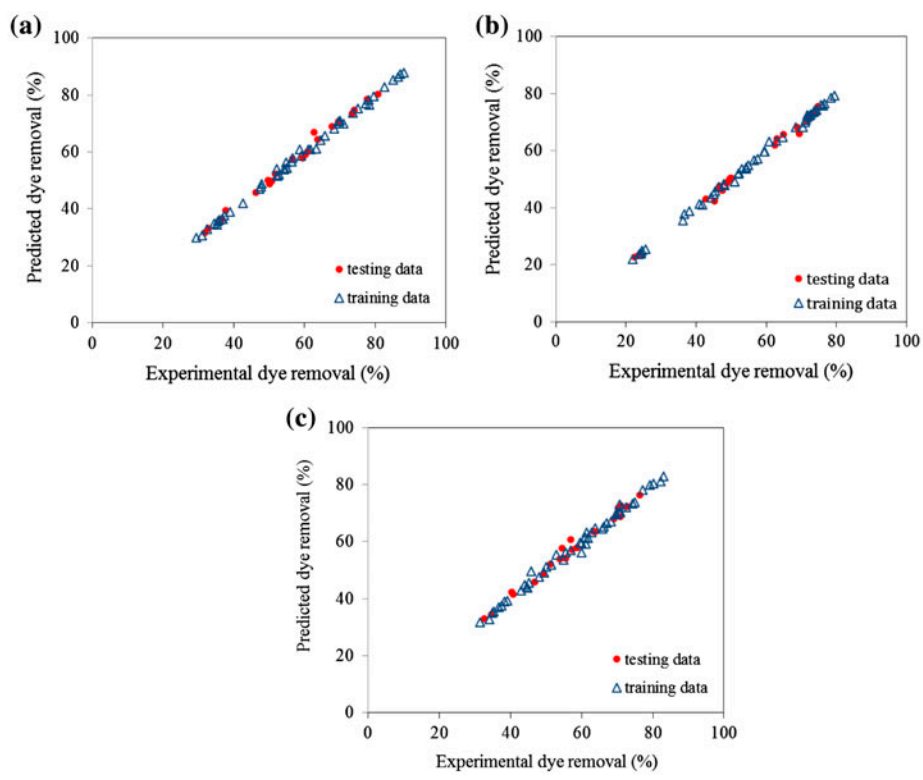

Fig. 4. Predicted dye removal vs. the experimental dye removal (a) BB41, (b) BR46, and (c) BR18.

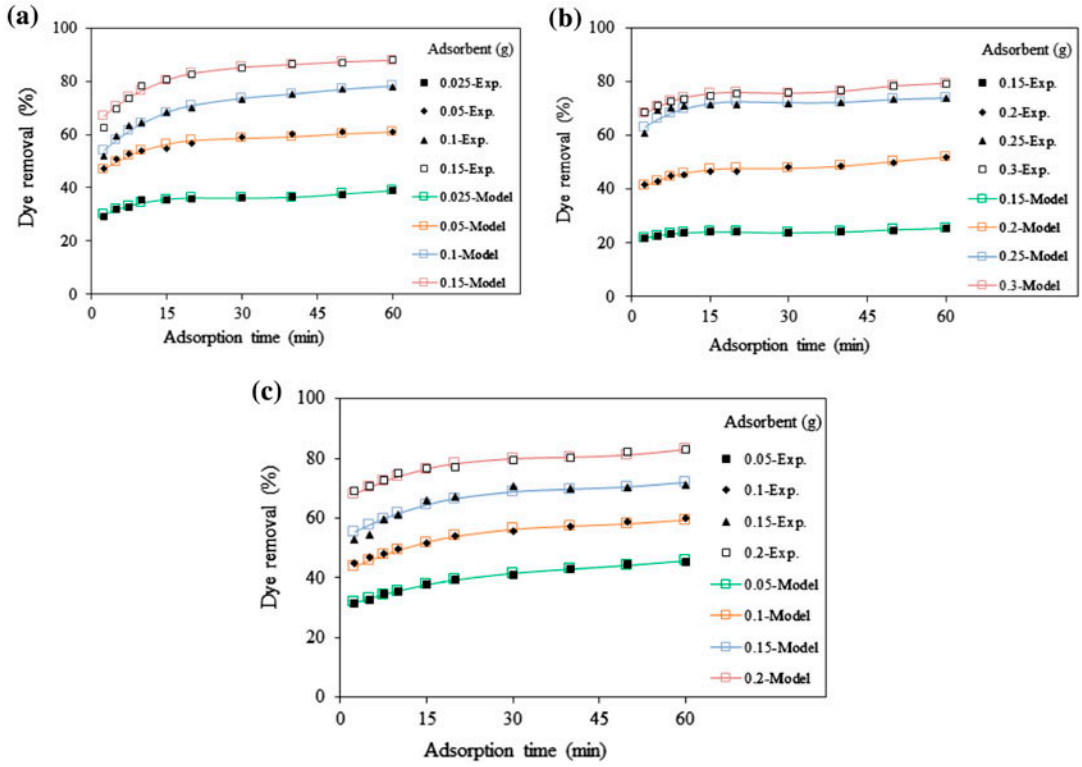

Fig. 5. Predicted and experimental dye removal vs. time at different adsorbent dosages (a) BB41, (b) BR46, and (c) BR18.

This is due to the overlapping or aggregation of adsorption sites, resulting in a decrease in total adsorbent surface area available to the dye and an increase in diffusion path length. Also, this figure confirms the agreement between the predicted dye removal values of LSSVM and experimental ones.

The plots of dye removal (%) vs. time (min) at different initial dye concentrations are shown in Fig. 6. For all dyes, the percentage of dye removal decreases with an increase in the initial dye concentration. The amount of the dye adsorbed onto the adsorbent increases with an increase in the initial dye concentration at a constant amount of adsorbent. This is due to the increase in the driving force of the concentration gradient with the higher initial dye concentration. At low initial dye concentration, the adsorption of dyes by MnO_2 nanoparticle is very intense and reaches equilibrium very quickly. In the case of lower dye concentrations, the ratio of initial number of dye moles to the available adsorption sites is low. In addition, it can be seen that the LSSVM model shows a good performance on prediction of the experimental data.

3.3. Adsorption isotherm

Adsorption isotherm presents how pollutant can be distributed between the liquid and solid phases at various equilibrium concentrations. Several isotherms such as the Langmuir, Freundlich, and Temkin models were studied in detail in order to investigate the design of an adsorption system to remove pollutants from wastewater because it is important to establish the most appropriate correlation for the equilibrium curve.

Langmuir isotherm assumes a uniform energy of adsorption and a single layer of adsorbed solute at a constant temperature. The Langmuir equation can be written as follows [28]:

$$C_e/q_e = 1/K_L Q_0 + C_e/Q_0 \quad (2)$$

where q_e, C_e, K_L, and Q_0 are the amount of dye adsorbed onto adsorbent at equilibrium (mg/g), the equilibrium concentration of dye solution (mg/L), the Langmuir constant (L/g), and the maximum adsorption capacity (mg/g), respectively.

The Freundlich isotherm is derived by assuming a non-uniform distribution of heat of adsorption over the surface. Freundlich isotherm can be expressed by [28]:

$$\log q_e = \log K_F + (1/n) \log C_e \quad (3)$$

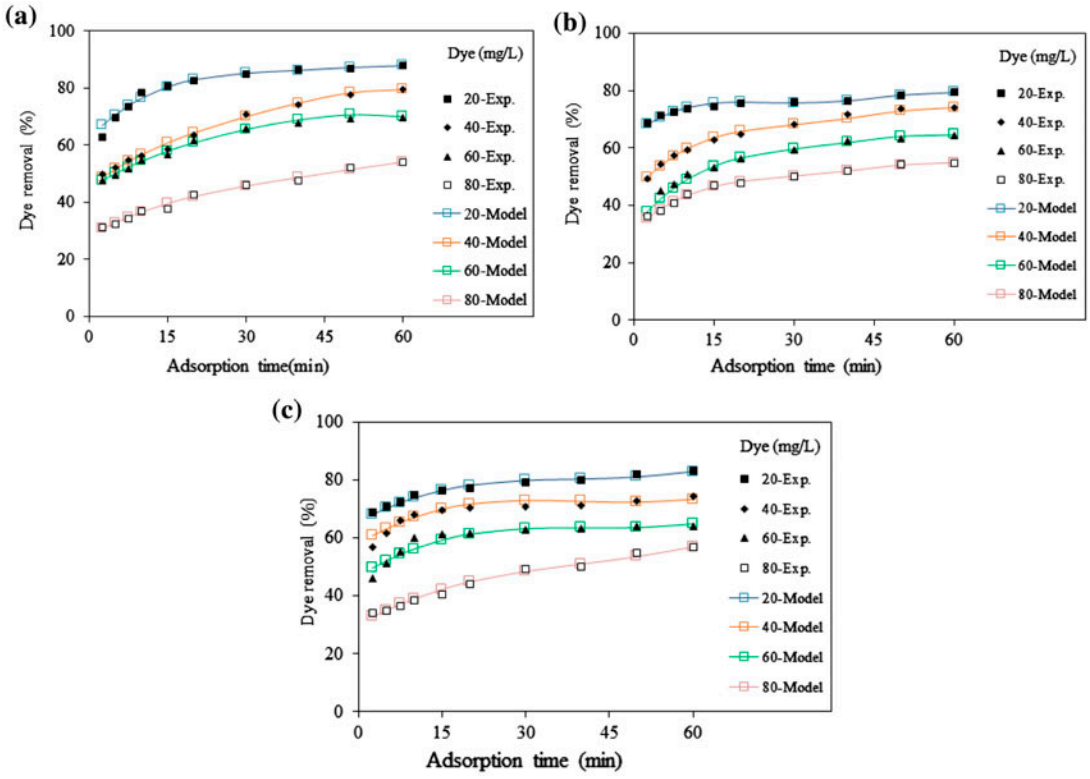

Fig. 6. Predicted and experimental dye removal vs. time at different initial dye concentrations (a) BB41, (b) BR46, and (c) BR18.

where K_F is the adsorption capacity at unit concentration and $1/n$ is adsorption intensity.

The Temkin isotherm is given as [29]:

$$q_e = B_1 \ln K_T + B_1 \ln C_e \quad (4)$$

where K_T is the equilibrium binding constant (L/mol) corresponding to the maximum binding energy and constant B_1 (RT/b) is related to the heat of adsorption. In addition, R and T are the gas constant (8.314 J/mol K) and the absolute temperature (K), respectively.

To study the applicability of the Langmuir, Freundlich, and Temkin isotherms for the dye adsorption onto adsorbent from dye solution at different adsorbent dosages, linear plots of C_e/q_e against C_e, log q_e vs. log C_e, and q_e vs. ln C_e were plotted. The values of Q_0, K_L, K_F, $1/n$, K_T, B_1, and R^2 are shown in Table 3.

The data show that isotherm of dye adsorption onto adsorbent does not conform to the Temkin isotherm. The R^2 values show that the dye removal isotherm for BB41, BR46, and BR18 follow the Freundlich, Langmuir, and Freundlich models, respectively.

3.4. Adsorption kinetic

Adsorption kinetic provides information about the mechanism of pollutant adsorption that is important for the efficiency of the process. Several models can be used to investigate the mechanism of adsorption onto an adsorbent. In order to investigate the mechanism of adsorption, characteristic constants of adsorption were determined using pseudo-first-order, pseudo-second-order, and intraparticle diffusion models.

Table 3
Linearized isotherm coefficients of dye removal at different adsorbent dosages

Langmuir			Freundlich			Tempkin		
Q_0	K_L	R^2	K_F	$1/n$	R^2	K_T	B_1	R^2
BB41								
141	0.0986	0.9481	17	0.6176	0.9897	1	30	0.9665
BR18								
101	0.0623	0.5009	9	0.6377	0.8735	1	20	0.8041
BR46								
8	0.3933	0.9542	24	0.3408	0.6767	196	4	0.6755

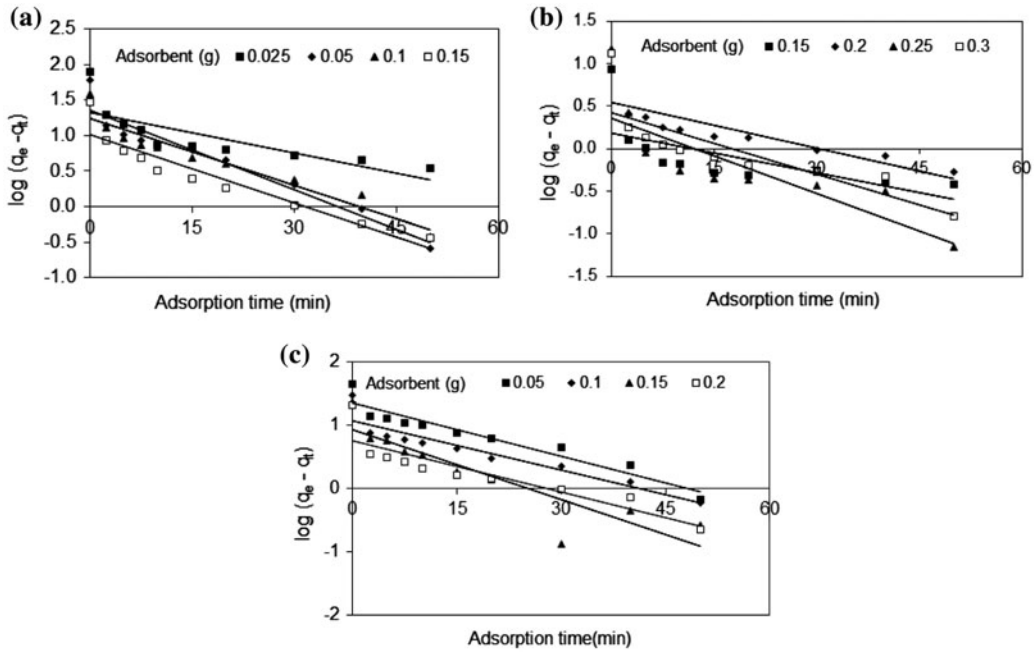

Fig. 7. Pseudo-first-order kinetic of dye removal (a) BB41, (b) BR46, and (c) BR18.

Table 4
Linearized kinetic coefficients of dye removal at different adsorbent dosages

			Pseudo-first-order			Pseudo-second-order				Intraparticle diffusion	
Dye	Adsorbent (g)	$(q_e)_{Exp.}$	$(q_e)_{Cal.}$	k_1	R^2	$(q_e)_{Cal.}$	k_2	R^2	k_p	I	R^2
BB41	0.025	78	21	0.0433	0.6462	78	0.0095	0.9987	2.5011	59	0.8421
	0.05	61	23	0.0861	0.9252	62	0.0110	0.9996	2.1328	46	0.9370
	0.10	40	17	0.0721	0.9197	40	0.0115	0.9993	1.9006	25	0.9230
	0.15	29	10	0.0739	0.8960	30	0.0219	0.9999	1.2203	21	0.8504
BR46	0.15	9	2	0.0359	0.4404	8	0.1482	0.9987	0.1474	7	0.8087
	0.20	13	4	0.0415	0.6621	13	0.0530	0.9982	0.3628	10	0.9608
	0.25	15	2	0.0679	0.6620	15	0.1273	0.9998	0.2626	13	0.5591
	0.30	13	3	0.0557	0.6832	13	0.0915	0.9996	0.2463	11	0.9389
BR18	0.05	45	22	0.0643	0.9091	46	0.0077	0.9977	2.3208	28	0.9908
	0.10	30	12	0.0594	0.8800	30	0.0158	0.9987	1.2336	21	0.9864
	0.15	24	8	0.0845	0.8023	24	0.0269	0.9997	1.0055	17	0.8603
	0.20	21	6	0.0624	0.8032	21	0.0398	0.9995	0.5501	17	0.9674

A linear form of pseudo-first-order equation is generally represented as follows [30–32]:

$$\log(q_e - q_t) = \log(q_e) - (k_1/2.303)t \quad (5)$$

where q_t and k_1 are the amount of adsorbed dye at time t (mg/g) and the equilibrium rate constant of pseudo-first-order kinetics (1/min), respectively.

The straight line plots of $\log(q_e - q_t)$ vs. t are represented in (Fig. 7). For the adsorption of BB41, BR18, and BR46 onto MnO_2 nanoparticle different dosages of adsorbent (0.025–0.3 g) have been tested to obtain the rate parameters. The k_1, q_e, and R^2 were calculated (Table 4).

Linear form of pseudo-second-order kinetic rate equation is expressed as [2,27–29]:

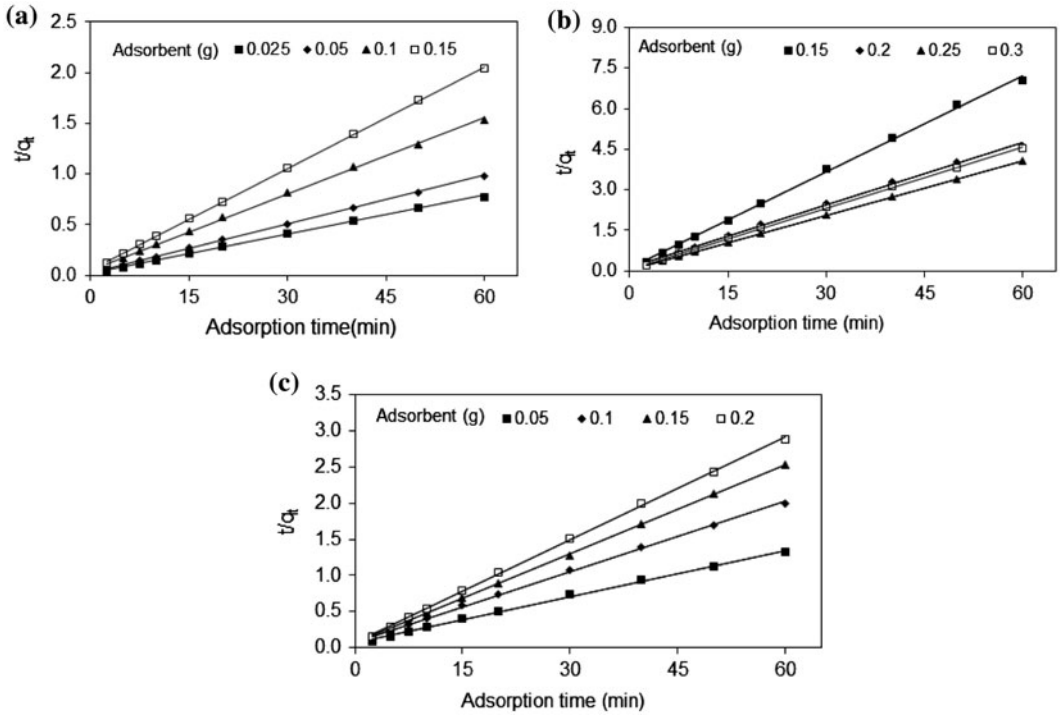

Fig. 8. Pseudo-second-order kinetic of dye removal (a) BB41, (b) BR46, and (c) BR18.

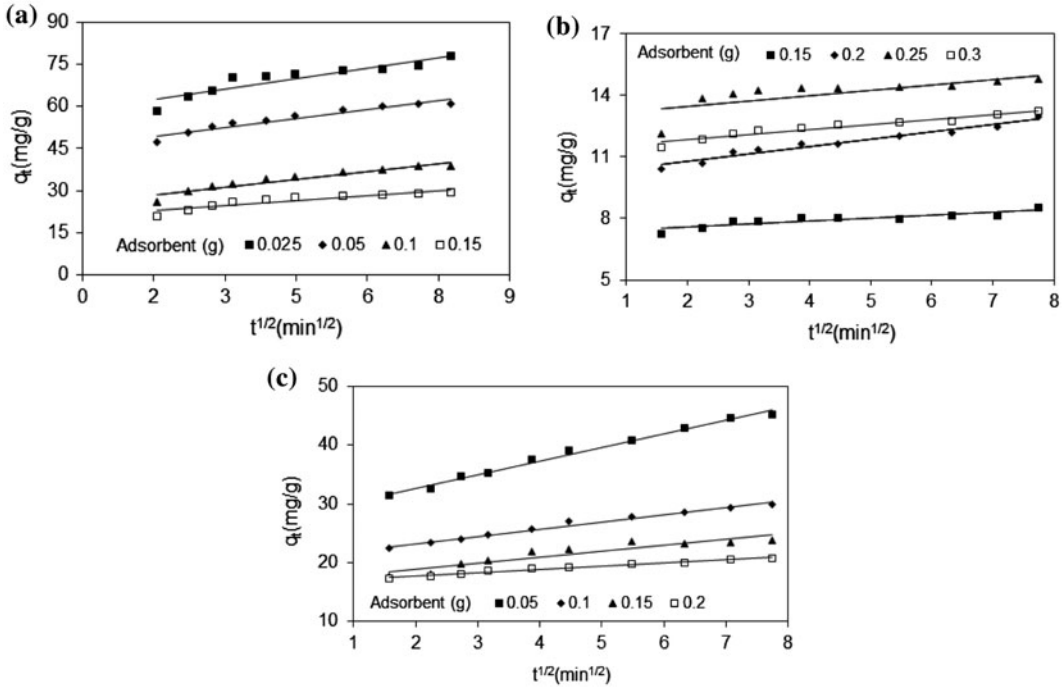

Fig. 9. Intraparticle diffusion kinetic of dye removal (a) BB41, (b) BR46, and (c) BR18.

$$t/q_t = 1/k_2 q_e^2 + t/q_e \quad (6)$$

where k_2 is the equilibrium rate constant of pseudo-second-order model (g/mg min).

To understand the applicability of the pseudo-second-order model, linear plots of t/q_t vs. t at different dosages of adsorbent (0.025–0.3 g) for the adsorption of dyes onto adsorbent were studied (Fig. 8). The k_2, q_e, and R^2 were calculated and given in Table 4.

The possibility of intraparticle diffusion resistance affecting adsorption was explored using the intraparticle diffusion model as [2,27–29]:

$$q_t = k_p t^{1/2} + I \quad (7)$$

where k_p and I are the intraparticle diffusion rate constant and intercept, respectively.

To understand the applicability of the intraparticle diffusion model for dye adsorption onto adsorbent at different adsorbent dosages, linear plot of q_t against $t^{1/2}$ was plotted (Fig. 9). The values of k_p, I, R^2, and the calculated q_e ($(q_e)_{Cal.}$) are shown in Table 4.

The linear fit between the t/q_t vs. contact time (t) and the values of R^2 for pseudo-second-order kinetic model show that the dye removal kinetic can be approximated as pseudo-second-order kinetic (Table 4). In addition, the experimental q_e ($(q_e)_{Exp.}$) values agree with the calculated ones ($(q_e)_{Cal.}$), obtained from the linear plots of pseudo-second-order model (Table 4).

4. Conclusion

In this paper, adsorption process as a simple and economical method was used to remove three cationic dyes from wastewater. For this purpose, MnO_2 nanoparticle as an adsorbent was synthesized in a short time and by a simple method. It was found that dye adsorption onto adsorbent followed Langmuir and Freundlich isotherms. Adsorption kinetic of dyes for this adsorbent conforms to pseudo-second-order kinetic. The results showed that adsorbent can be proposed as a suitable adsorbent for cationic dye removal. Based on graphical plots and values of R^2, LSSVM was found to be appropriate as a powerful tool for modeling of adsorption process in our system.

References

[1] N.M. Mahmoodi, Binary catalyst system dye degradation using photocatalysis, Fibers Polym. 15 (2014) 273–280.
[2] N.M. Mahmoodi, Synthesis of magnetic carbon nanotube and photocatalytic dye degradation ability, Environ. Monit. Assess. 186 (2014) 5595–5604.
[3] N.M. Mahmoodi, Photodegradation of dyes using multiwalled carbon nanotube and ferrous ion, J. Environ. Eng. 139 (2013) 1368–1374.
[4] T. Zhu, J.S. Chen, X.W. Lou, Highly efficient removal of organic dyes from waste water using hierarchical NiO spheres with high surface area, J. Phys. Chem. C 116 (2012) 6873–6878.
[5] N.M. Mahmoodi, Photocatalytic ozonation of dyes using multiwalled carbon nanotube, J. Mol. Catal. A: Chem. 366 (2013) 254–260.
[6] E. Forgacs, T. Cserháti, G. Oros, Removal of synthetic dyes from wastewaters: A review, Environ. Int. 30 (2004) 953–971.
[7] H. Sun, L. Cao, L. Lu, Magnetite/reduced graphene oxide nanocomposites: One step solvothermal synthesis and use as a novel platform for removal of dye pollutants, Nano Res. 4 (2011) 550–562.
[8] G.K. Ramesha, A. Vijaya Kumara, H.B. Muralidhara, S. Sampath, Graphene and graphene oxide as effective adsorbents toward anionic and cationic dyes, J. Colloid Interface Sci. 361 (2011) 270–277.
[9] K. Singh, S. Arora, Removal of synthetic textile dyes from wastewaters: A critical review on present treatment technologies, Crit. Rev. Env. Sci. Technol. 41 (2014) 807–878.
[10] N.M. Mahmoodi, Surface modification of magnetic nanoparticle and dye removal from ternary systems, J. Ind. Eng. Chem. 27 (2015) 251–259.
[11] M.T. Yagub, T.K. Sen, S. Afroze, H.M. Ang, Dye and its removal from aqueous solution by adsorption: A review, Adv. Colloid Interface Sci. 209 (2014) 172–184.
[12] N.M. Mahmoodi, Manganese ferrite nanoparticle: Synthesis, characterization and photocatalytic dye degradation ability, Desalin. Water Treat. 53 (2015) 84–90.
[13] S.T. Ong, P.S. Keng, W.N. Lee, S.T. Ha, Y.T. Hung, Dye waste treatment, Water 3 (2011) 157–176.
[14] N.M. Mahmoodi, Zinc ferrite nanoparticle as a magnetic catalyst: Synthesis and dye degradation, Mater. Res. Bull. 48 (2013) 4255–4260.
[15] N.M. Mahmoodi, M. Bashiri, S.J. Moeen, Synthesis of nickel–zinc ferrite magnetic nanoparticle and dye degradation using photocatalytic ozonation, Mater. Res. Bull. 47 (2012) 4403–4408.
[16] A.K. Verma, R.R. Dash, P. Bhunia, A review on chemical coagulation/flocculation technologies for removal of colour from textile wastewaters, J. Environ. Manage. 93 (2012) 154–168.
[17] A. Dalvand, M. Gholami, A. Joneidi, N.M. Mahmoodi, Dye removal, energy consumption and operating cost of electrocoagulation of textile wastewater as a clean process, Clean—Soil Air Water 39 (2011) 665–672.
[18] A. Vázquez-Olmos, R. Redón, G. Rodríguez-Gattorno, M.E. Mata-Zamora, F. Morales-Leal, A.L. Fernández-Osorio, J.M. Saniger, One-step synthesis of Mn3O4 nanoparticles: Structural and magnetic study, J. Colloid Interface Sci. 291 (2005) 175–180.
[19] S. Liang, F. Teng, G. Bulgan, R. Zong, Y. Zhu, Effect of phase structure of MnO_2 nanorod catalyst on the activity for CO oxidation, J. Phys. Chem. C 112 (2008) 5307–5315.
[20] D. Zhao, X. Yang, H. Zhang, C. Chen, X. Wang, Effect of environmental conditions on Pb(II) adsorption on β -MnO_2, Chem. Eng. J. 164 (2010) 49–55.

[21] R. Chen, J. Yu, W. Xiao, Hierarchically porous MnO_2 microspheres with enhanced adsorption performance, J. Mater. Chem. A 1 (2013) 11682–11690.
[22] J.A. Suykens, J. Vandewalle, Least squares support vector machine classifiers, Neural Process. Lett. 9 (1999) 293–300.
[23] J.A. Suykens, Support vector machines: A nonlinear modelling and control perspective, Eur. J. Control 7 (2001) 311–327.
[24] X. Yunrong, J. Liangzhong, Water quality prediction using LS-SVM and particle swarm optimization, Second International Workshop on Knowledge Discovery and Data Mining (2009) 900–904.
[25] N.M. Mahmoodi, M. Arabloo, J. Abdi, Laccase immobilized manganese ferrite nanoparticle: Synthesis and LSSVM intelligent modeling of decolorization, Water Res. 67 (2014) 216–226.
[26] M. Ghaedi, A. Ghaedi, M. Hossainpour, A. Ansari, M. Habibi, A. Asghari, Least square-support vector (LS-SVM) method for modeling of methylene blue dye adsorption using copper oxide loaded on activated carbon: Kinetic and isotherm study, J. Ind. Eng. Chem. 20 (2014) 1641–1649.
[27] N. Xin, X. Gu, H. Wu, Y. Hu, Z. Yang, Application of genetic algorithm-support vector regression (GA-SVR) for quantitative analysis of herbal medicines, J. Chemom. 26 (2012) 353–360.
[28] L. Fan, C. Luo, M. Sun, H. Qiu, X. Li, Synthesis of magnetic β-cyclodextrine- chitosan/graphene oxide as nanoadsorbent and its application in dye adsorption and removal, Colloids Surf. B 103 (2013) 601–607.
[29] N.M. Mahmoodi, B. Hayati, M. Arami, Kinetic, equilibrium and thermodynamic studies of ternary system dye removal using a biopolymer, Ind. Crop. Prod. 35 (2009) 295–301.
[30] N.M. Mahmoodi, Synthesis of core-shell magnetic adsorbent nanoparticle and selectivity analysis for binary system dye removal, J. Ind. Eng. Chem. 20 (2014) 2050–2058.
[31] N.M. Mahmoodi, Synthesis of amine-functionalized magnetic ferrite nanoparticle and its dye removal ability, J. Environ. Eng. 139 (2013) 1382–1390.
[32] N.M. Mahmoodi, Dendrimer functionalized nanoarchitecture: Synthesis and binary system dye removal, J. Taiwan Inst. Chem. Eng. 45 (2014) 2008–2020.